Chapter 11

The Cyclogenesis and Decay of Typhoon Damrey

X. San Liang and Lan Wang

Additional information is available at the end of the chapter

http://dx.doi.org/10.5772/intechopen.80018

Abstract

The cyclogenesis of typhoons has been a continuing challenge in dynamic meteorology. In this study, we use a recently developed methodology, namely, multiscale window transform (MWT), together with the MWT-based localized multiscale energy and vorticity analysis and the theory of canonical transfer, to investigate the formation, maintenance, and decay of the typhoon Damrey, a rarely seen tropical storm of higher-latitude origin. The atmospheric fields are first reconstructed onto three scale subspaces or scale windows: large-scale window, tropical cyclone-scale window, and cumulus convection-scale window. On the cyclone-scale window, Damrey is found right along the edge of the subtropical high. It is generated due to a strong barotropic instability in the lower troposphere, but its subsequent rapid amplification is, however, related to a baroclinic instability in the upper troposphere. Damrey begins to decay before landfall, right over East China Sea at the mouth of Yangtze River, where a strong inverse cascade center resides and transfers the cyclone-scale energy backward to the large-scale window.

Keywords: typhoon Damrey, twin typhoon, multiscale window transform, multiscale energetics, barotropic/baroclinic instability, canonical transfer

1. Introduction

A typhoon is a tropical cyclone that develops in the Northwestern Pacific basin and has wind speed of at least 64 knots (118 km/h). It is among the major meteorological phenomena that bring about natural hazards to coastal regions. For the densely populated coastal province Jiangsu, China, it has been recorded that since 1950, there have been landed 14 tropical cyclones (tropical storm level or higher). The typhoon Damrey that landed in Xiangshui, Jiangsu, on August 2, 2012, in particular, has inflicted a heavy damage to the region and its surrounding Chinese provinces such as Fujian, Zhejiang, and Shandong and has severely

affected 1.7 million residents, leaving 932,000 homeless. In this study, we present an analysis of the cyclogenesis and decay of Damrey.

Damrey is unique in that it does not originate between 20°N and 20°S, just like most of tropical cyclones [1]; rather, it is born at a relatively high latitude (a rare event). Moreover, it is actually a part of a twin typhoon. The other part, Saola, which appeared on the same day (July 28) as Damrey over the Western Pacific Ocean, also landed on China, but only several hours earlier. Shown in **Figure 1** are the paths of them. From it, Saola forms over the ocean east of the Philippines, while Damrey forms at a latitude as high as 24.8°N. On August 2, Damrey landed directly on Jiangsu, making the most powerful typhoon that has ever landed on China from north of Yangtze River. As it moves westward, Damrey becomes weakened, but its twin, Saola, becomes stronger. After landing, it turns northward, and then decays rapidly until it completely disappears.

This important meteorological phenomenon, however, has not caught enough attention from dynamic meteorologists. So far, the only report is by Wang and Liang [2], which we will be introduced henceforth.

Cyclogenesis is closely related to multiscale interactions. It has been reported (e.g., [3], and the references therein) that tropical cyclogenesis may be triggered by mesoscale processes under

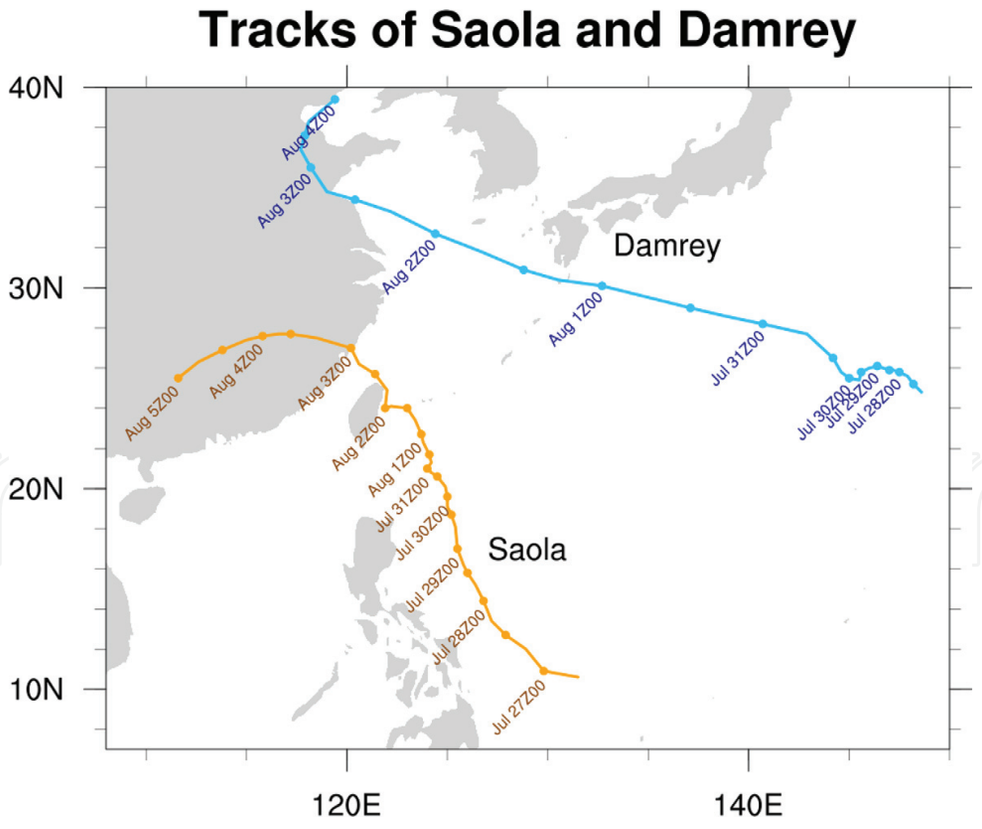

Figure 1. The paths of the twin typhoon Damrey and Saola (data courtesy of China Meteorological Administration).

the control of large-scale systems. Examples include the easterly waves in the Atlantic [4, 5], the monsoon troughs in the Pacific [1, 6–10], Madden-Julian oscillation (MJO) [11–14], tropical upper tropospheric troughs [15–17], and so forth. However, tropical cyclogenesis has seldom been investigated through multiscale energetics diagnosis, a natural approach to multiscale interactions, except a few studies such as Ooyama [18], Papin [19], Duan and Wu [20], etc. A reason is the lack of an appropriate methodology; a particularly critical issue here is: the traditional formalisms of the energy transfers between different scales cannot have the multiscale interaction faithfully represented. Recently, Wang and Liang [2] presented a study from this angle, using a newly developed functional analysis tool, multiscale window transform (MWT), and the MWT-based localized multiscale energy and vorticity analysis (MS-EVA). This chapter provides an exposition of what they have obtained, with some parts expanded as needed. The following is a brief introduction of the new methodology, and a theory of canonical transfer. We first apply it to reconstruct the two cyclones (Section 5), and then analyze the underlying dynamical processes (Section 6). Section 7 is a summary of the results; also in the same section, we make a brief comparison of some observations with the existing theories.

2. Multiscale window transform (MWT), canonical transfer, and localized multiscale energy and vorticity analysis (MS-EVA)

2.1. Multiscale window transform

As is well known, multiscale energetics formulated with time mean do not have information in time, and those formulated with zonal mean lose information in longitude, etc. Obviously, such formalisms cannot be used to study the energy burst processes such as cyclogenesis, which are in nature localized in space and time. During the past decades, a common practice is simply to remove the time mean in a Reynolds decomposition-based formalism. This is, unfortunately, conceptually wrong; we will soon see why below. A "more sophisticated" and widely adopted practice is to use filtering to replace the time averaging in the above formalism. For example, a field $u(t)$ (the spatial dependence is suppressed for clarity) can be decomposed with a filter into a slowly varying part $\overline{u}$ and a fast varying eddy part u'. Now both of these parts have time information reserved, and this is precisely why filtering has been widely used. While mathematically this technique is indeed advantageous, however, a very basic physical question arises: What are the energies with respect to the resulting filtered fields? Particularly, we know for a time invariant $\overline{u}$ in the decomposition $u(t) = \overline{u} + u'(t)$, the eddy energy is $\overline{[u'(t)]^2}$; now if $\overline{u}$ is time variable, what is the eddy energy then?

During the past 2–3 decades, a common practice in the literature is simply to take it as $[u'(t)]^2$. However, the result is by no means this trivial; in fact, this is a very fundamental problem.

To illustrate, suppose we have a simple Fourier expansion

$$u(t) = \overline{u}(t) + u'(t) = [a_0 \cos t + b_0 \sin t] + [a_1 \cos 100t + b_1 \sin 100t] \tag{1}$$

where the subscripts 0 and 1 represent the slow- and fast-scale processes, respectively. Now what are the energies for these processes? By the common practice they are simply taken as

$$[\overline{u}(t)]^2 = [a_0 \cos t + b_0 \sin t]^2 \text{ and } \left[u'(t)\right]^2 = [a_1 \cos 100t + b_1 \sin 100t]^2. \tag{2}$$

Unfortunately, this is conceptually wrong! We know here the results should be, respectively,

$$a_0^2 + b_0^2 \text{ and } a_1^2 + b_1^2, \tag{3}$$

which are functions of the Fourier coefficients in phase space, not the reconstructions or filtered parts in physical space!

So, multiscale energy is a concept in phase space, which is related to its physical space counterpart through the Parseval relation in functional analysis. It is actually the square of the norm of a field variable, or, physically, it is the Fourier transform of an autocorrelation function (e.g., [21]). In the above example, when $\overline{u}$ is time invariant, one can easily prove $a_1^2 + b_1^2 = \overline{[u'(t)]^2}$, just as that with the Reynolds decomposition. From this, one also sees why the time averaging in the classical energetic formalism cannot be removed to retain the time variability; otherwise, the resulting energetics does not make sense in physics.

It is, therefore, a rather complex and profound problem to have the local energy of a time-dependent filtered field faithfully represented. This even has been an impossible task until filter banks and wavelets are connected [22], and has just been systematically addressed by Liang and Anderson [23] in the development of multiscale window transform (MWT).

MWT is an apparatus that helps to decompose a function space into a direct sum of orthogonal subspaces, each with an exclusive range of scales (represented by wavelet scale levels). Such a subspace is termed a *scale window*, or simply a window. MWT is originally developed for representing the energies on the resulting multiple scale windows, in order to make multiscale energetics analysis possible. Liang and Anderson [23] find that, for some specially constructed orthogonal filters, there exists a transfer-reconstruction pair, just as the Fourier transform and inverse Fourier transform (Note here, *orthogonality* is crucial; otherwise, energy cannot even be defined.) This pair is the very MWT and its peer, namely, multiscale window reconstruction (MWR). Loosely speaking, the MWR of a series S(t) results in a filtered series, while the corresponding MWT coefficients can give the energy of that filtered series. This is in contrast to the traditional filters; their outputs are fields in physical space, and, as argued above, cannot be used to represent multiscale energy, which is a concept in phase space.

In MWT, a scale window is demarcated on the wavelet spectrum by two scale levels, or window bounds. For a time series with a duration τ, a scale level j corresponds to a period $2^{-j}\tau$.

Obviously, the number of time steps need to be a power of 2. In this study, we will need three scale windows, which are bounded above by three scale levels: j_0, j_1, and j_2. Alternatively, $2^{-j_0}\tau$, $2^{-j_1}\tau$, and $2^{-j_2}\tau$ are the time scale bounds. For convenience, we will, henceforth, refer to them as **large-scale window**, **tropical cyclone-scale window (or simply cyclone window)**, and **cumulus convection-scale window (or convection window)**, and will denote them by $\varpi = 0, 1, 2$, respectively.

Given a time series $\{S(t)\}$, application of MWT yields the transform coefficient, written $\widehat{S}_n^{\sim\varpi}$ [$\widehat{(\cdot)}_n^{\sim\varpi}$ denotes MWT on window ϖ at time step n]; likewise, application of MWR results in a reconstruction on window ϖ, written $\mathrm{S}^{\sim\varpi}(t)$. Here, the tilde in the superscript indicates that the MWT is for a range of scales, rather than for a specific scale as in the other transforms (such as wavelet transform). It is also used to avoid confusion with notations that do not carry meaning of transform and/or reconstruction (We will see such notations later in the energetics.) It has been shown that the energy on window ϖ is proportional to $\left(\widehat{S}_n^{\sim\varpi}\right)^2$ (Note it is by no means as trivial as $[\mathrm{S}^{\sim\varpi}(t)]^2$, i.e., the square of the filtered field!). For a dry atmosphere, the multiscale kinetic energy (KE) and available potential energy (APE) are then, up to some proportionality, $\widehat{\mathbf{v}}_h^{\sim\varpi}\cdot\widehat{\mathbf{v}}_h^{\sim\varpi}$ and $\left(\widehat{\mathrm{T}}^{\sim\varpi}\right)^2$, respectively, where $\mathbf{v}$ is velocity, T is temperature, and the subscript h indicates horizontal component. In the following, we will see more details.

2.2. Multiscale energetics and Lorenz cycle

Following Liang [24], we consider the primitive equations in an isobaric coordinate frame:

$$\frac{\partial \mathbf{v}_h}{\partial t} + \mathbf{v}_h\cdot\nabla_h\mathbf{v}_h + \omega\frac{\partial \mathbf{v}_h}{\partial p} + f\mathbf{k}\times\mathbf{v}_h = -\nabla_h\Phi + \mathbf{F}_{m,p} + \mathbf{F}_{m,h}, \tag{4}$$

$$\frac{\partial \Phi}{\partial p} = -\alpha, \tag{5}$$

$$\nabla_h\cdot\mathbf{v}_h + \frac{\partial \omega}{\partial p} = 0, \tag{6}$$

$$\frac{\partial T}{\partial t} + \mathbf{v}_h\cdot\nabla_h\mathrm{T} + \omega\frac{\partial T}{\partial p} + \omega\overline{\alpha}\frac{L-L_d}{g} + \omega\alpha\frac{L-L_d}{g} = \frac{\dot{q}_{net}}{c_p}, \tag{7}$$

$$\alpha = \frac{R}{p}T \tag{8}$$

where L is the lapse rate and L_d the lapse rate for dry air, and the overbar stands for mean over time and over the horizontal isobaric plane. The other notations are conventional. Note here Φ (geopotential) and α (specific volume) are anomalies; their time averages have been presubtracted. From Eqs. (4)–(8), Liang [24] shows that the multiscale KE and APE equations are, for windows ϖ (= 0, 1, 2),

$$\frac{\partial K^{\varpi}}{\partial t} + \nabla\cdot\mathbf{Q}_K^{\varpi} = \Gamma_K^{\varpi} - \nabla\cdot\mathbf{Q}_P^{\varpi} - b^{\varpi} + \mathrm{F}_{K,p}^{\varpi} + \mathrm{F}_{K,h}^{\varpi}, \tag{9}$$

$$\frac{\partial A^{\varpi}}{\partial t} + \nabla\cdot\mathbf{Q}_A^{\varpi} = \Gamma_A^{\varpi} + b^{\varpi} + \mathrm{S}_A^{\varpi} + \mathrm{F}_A^{\varpi} \tag{10}$$

The explanations and expressions for these terms are listed in **Table 1**. Note here the time step n has been suppressed for simplicity. Among these terms, the $\mathbf{\Gamma}$ terms represent transfers between different scale windows; they are very different from those in classical formalisms. Particularly, there is an interesting property, i.e.,

$$\sum\nolimits_{\varpi}\left(\sum\nolimits_{n}\Gamma_n^{\varpi}\right) = 0 \tag{11}$$

(now n is supplied) as first shown in Liang and Robinson [25] and later on rigorously proved (see [24]). Physically, this means that the energy transfer is a mere redistribution of energy among the scale windows, without generating or destroying energy as a whole. This property, though simply stated, does not hold in previous time decomposition-based or Lorenz-type energetics formalisms (see below). To distinguish, such as transfer is termed "*canonical transfer.*" A canonical transfer has a Lie bracket form that satisfies the Jacobian identity, reminiscent of the Poisson bracket in Hamiltonian mechanics; see Liang [24] for details (Note it is not the detailed balance relation in the Saltzman-type or space decomposition-based energetics formalisms, which results from the interaction analysis to be shown below).

To see how a canonical transfer differs from the energy transfer in classical energetics formalisms, we consider a passive tracer T (may be any scalar field; need not be temperature) in an incompressible flow, and neglect all other processes but for advection:

Symbol	Expression	Physical meaning
K^{ϖ}	$\frac{1}{2}\widehat{\mathbf{v}}_h^{\sim\varpi}\cdot\widehat{\mathbf{v}}_h^{\sim\varpi}$	KE on scale window ϖ
$\boldsymbol{Q}_K^{\varpi}$	$\frac{1}{2}\widehat{(\mathbf{v}\mathbf{v}_h)}^{\sim\varpi}\cdot\widehat{\mathbf{v}}_h^{\sim\varpi}$	Flux of KE on window ϖ
Γ_K^{ϖ}	$\frac{1}{2}\left[\widehat{(\mathbf{v}\mathbf{v}_h)}^{\sim\varpi} : \nabla\widehat{\mathbf{v}}_h^{\sim\varpi} - \nabla\cdot\widehat{(\mathbf{v}\mathbf{v}_h)}^{\sim\varpi}\cdot\widehat{\mathbf{v}}_h^{\sim\varpi}\right]$	Canonical transfer of KE to window ϖ
$\boldsymbol{Q}_P^{\varpi}$	$\widehat{\mathbf{v}}^{\sim\varpi}\widehat{\Phi}^{\sim\varpi}$	Pressure flux
b^{ϖ}	$\widehat{\omega}^{\sim\varpi}\widehat{\alpha}^{\sim\varpi}$	Buoyancy conversion
A^{ϖ}	$\frac{1}{2}c\left(\widehat{\mathrm{T}}^{\sim\varpi}\right)^2$, $c=\frac{g}{\overline{T}(g/C_p-L)}$	APE on scale window ϖ
$\boldsymbol{Q}_A^{\varpi}$	$\frac{1}{2}c\widehat{\mathrm{T}}^{\sim\varpi}\widehat{(\mathbf{v}\mathrm{T})}^{\sim\varpi}$	Flux of APE on window ϖ
Γ_A^{ϖ}	$\frac{c}{2}\left[\widehat{(\mathbf{v}\mathrm{T})}^{\sim\varpi}\cdot\nabla\widehat{\mathrm{T}}^{\sim\varpi} - \widehat{\mathrm{T}}^{\sim\varpi}\nabla\cdot\widehat{(\mathbf{v}\mathrm{T})}^{\sim\varpi}\right]$	Canonical transfer of APE to window ϖ
S_A^{ϖ}	$\frac{1}{2}\widehat{\mathrm{T}}^{\sim\varpi}\widehat{(\omega T)}^{\sim\varpi}\frac{\partial c}{\partial p}+\frac{1}{\overline{T}}\widehat{\omega\alpha}^{\sim\varpi}$	Apparent source/sink (usually negligible)

If total energetics (in W) are to be computed, the resulting integrals with respect to (x, y, p) should be divided by g. Besides, all terms are to be multiplied by 2^{j_2}, which is omitted for notational simplicity.

Table 1. The energetic terms in Eqs. (9) and (10).

$$\frac{\partial T}{\partial t} + \nabla\cdot(\mathbf{v}T) = 0 \tag{12}$$

In a traditional Reynolds decomposition $\bar{\mathbf{v}}\bar{T}^2 2$ framework, its decomposed equations are

$$\frac{\partial \overline{T}}{\partial t} + \nabla\cdot\left(\overline{\mathbf{v}}\,\overline{T} + \overline{\mathbf{v}'T'}\right) = 0, \tag{13}$$

$$\frac{\partial T'}{\partial t} + \nabla\cdot\left(\mathbf{v}'\overline{T} + \overline{\mathbf{v}}T' + \mathbf{v}'T' - \overline{\mathbf{v}'T'}\right) = 0, \tag{14}$$

Multiplying (13) by $\overline{T}$ and (14) by T′, followed by an averaging, one arrives at the evolutions of the mean energy and eddy energy (variance) (e.g., [26])

$$\frac{\partial \overline{T}^2/2}{\partial t} + \nabla\cdot\left(\frac{\overline{\mathbf{v}}\,\overline{T'^2}}{2}\right) = -\overline{T}\nabla\cdot(\overline{\mathbf{v}'T'}), \tag{15}$$

$$\frac{\partial \overline{T'^2/2}}{\partial t} + \nabla\cdot\left(\frac{\overline{\mathbf{v}T'^2}}{2}\right) = -\overline{\mathbf{v}'T'}\cdot\nabla\overline{T} \tag{16}$$

The terms in divergence form are generally understood as the transports of the mean and eddy energies, and those on the right-hand side as the respective energy transfers during the mean-eddy interaction. Particularly, when T is a velocity component, the right side of (16), $\mathrm{R} = -\overline{\mathbf{v}'T'}\cdot\nabla\overline{T}$, has been interpreted as the rate of energy extracted by Reynolds stress against the mean profile; in the context of turbulence research, it is also referred to as the "rate of the turbulence production" [26]. It has been extensively utilized in geophysical fluid dynamics for the explanation of the phenomena such as cyclogenesis, eddy shedding, etc. However, Holopainen [27] and Plumb [28] have argued that the transport-transfer separation is ambiguous, and hence the resulting transfer is physically not robust. Moreover, Eqs. (15) and (16) do not, in general, sum to zero on the right-hand side. This is not what one would expect of an energy transfer, which by physical intuition should be a redistribution of energy among scale/scale windows and should not generate nor destroy energy as a whole.

With the MS-EVA formalism, the above are not issues any more. In this special case, the energy equations (9) and (10) are reduced to (see [24]),

$$\frac{\partial \overline{T}^2/2}{\partial t} + \nabla\cdot\left(\frac{1}{2}\overline{\mathbf{v}}\,\overline{T}^2 + \frac{1}{2}\overline{T}\,\overline{\mathbf{v}'T'}\right) = -\Gamma, \tag{17}$$

$$\frac{\partial \overline{T'^2/2}}{\partial t} + \nabla\cdot\left(\frac{1}{2}\overline{\mathbf{v}T'^2} + \frac{1}{2}\overline{T}\,\overline{\mathbf{v}'T'}\right) = \Gamma, \tag{18}$$

where $\Gamma = \frac{1}{2}\left\{\overline{T}\nabla\cdot\left(\overline{\mathbf{v}'T'}\right) - \left(\overline{\mathbf{v}'T'}\right)\cdot\nabla\overline{T}\right\}$. Now, one can see that the right-hand side is balanced, in contrast to Eqs. (15) and (16). We hence call this Γ a "canonical transfer." As shown

by Liang [24], it has a Lie bracket form. Previously, Liang and Robinson [29] illustrate that, for a benchmark hydrodynamic instability model whose instability structure is analytically known, the traditional Reynolds stress extraction $R = -\overline{\mathbf{v}'T'}\cdot\nabla\overline{T}$ does not give the correct source of instability, while Γ does.

The MS-EVA equations (9) and (10) are thus fundamentally different from the classical ones. By collecting the energetic terms, one sees that a local Lorenz cycle is composed of four types of processes: transport (divergence of energy flux), canonical transfer, buoyancy conversion, and dissipation/diffusion. Obviously, the first three are conservative: a transport vanishes if integrated over a closed domain, a canonical transfer vanishes if summarized over windows and locations, while a buoyancy conversion disappears if the total mechanical energy, i.e., KE + APE, is considered. In **Figure 2,** these processes are schematized with a three-window decomposition.

Note that a canonical transfer to a window ϖ may involve contributions from different windows; we need to differentiate them to trace the dynamical source. As an example, we consider the cyclone window ($\varpi = 1$). The energy transferred to it can be from window 0, 2, and even itself $\varpi = 1$. Observe that both Γ_K^1 and Γ_A^1 **(**cf. **Table 1)** can be expressed as a linear combination of terms in the following triple product form:

$$\Gamma_n^1 = \hat{\mathscr{R}}_n^{-1}\widetilde{(pq)}_n^{-1} \tag{19}$$

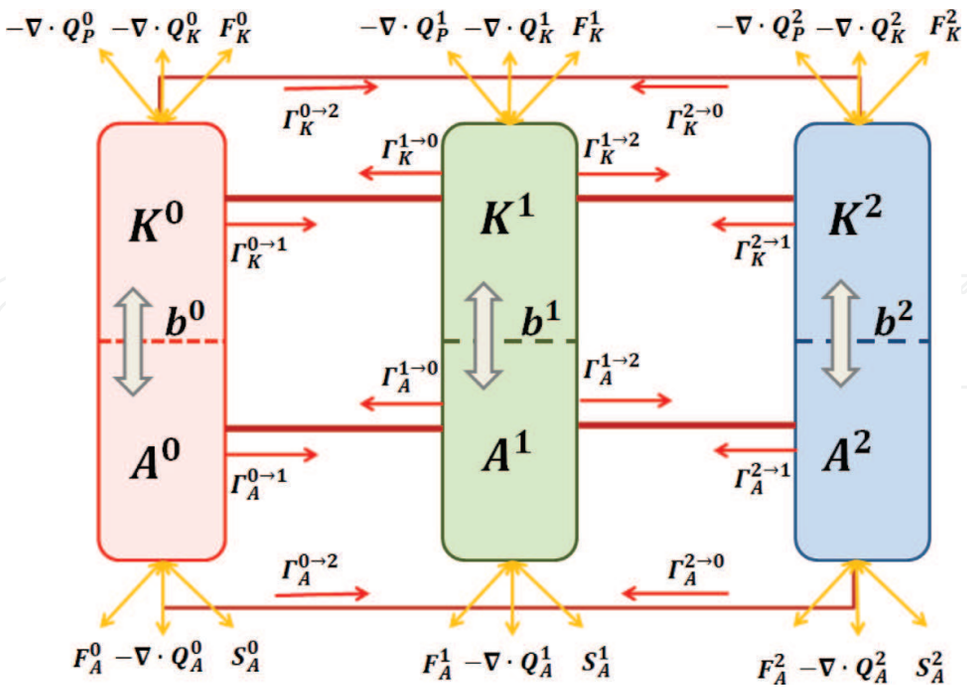

Figure 2. Multiscale energy pathway for a three-window decomposition (the scale windows are denoted in the superscripts as 0, 1, and 2, respectively).

It then suffices to consider Γ_n^1 only. As established in Liang [24], it can be decomposed as

$$\begin{aligned}\Gamma_n^1 = {} & \hat{\mathscr{R}}_n^{\sim 1}\left[(\widehat{p^{\sim 0}q^{\sim 0}})_n^{\sim 1} + (\widehat{p^{\sim 0}q^{\sim 1}})_n^{\sim 1} + (\widehat{p^{\sim 1}q^{\sim 0}})_n^{\sim 1}\right] \\ & + \hat{\mathscr{R}}_n^{\sim 1}\left[(\widehat{p^{\sim 1}q^{\sim 2}})_n^{\sim 1} + (\widehat{p^{\sim 2}q^{\sim 1}})_n^{\sim 1} + (\widehat{p^{\sim 2}q^{\sim 2}})_n^{\sim 1}\right] \\ & + \hat{\mathscr{R}}_n^{\sim 1}\left[(\widehat{p^{\sim 0}q^{\sim 2}})_n^{\sim 1} + (\widehat{p^{\sim 2}q^{\sim 0}})_n^{\sim 1}\right] \\ & + \hat{\mathscr{R}}_n^{\sim 1}(\widehat{p^{\sim 1}q^{\sim 1}})_n^{\sim 1}.\end{aligned} \tag{20}$$

where the first row on the right-hand side, $\hat{\mathscr{R}}_n^{\sim 1}\left[(\widehat{p^{\sim 0}q^{\sim 0}})_n^{\sim 1} + (\widehat{p^{\sim 0}q^{\sim 1}})_n^{\sim 1} + (\widehat{p^{\sim 1}q^{\sim 0}})_n^{\sim 1}\right] \equiv \Gamma^{0\to 1}$ is the canonical energy transfer from window 0 to window 1. The second row, denoted by $\Gamma^{2\to 1}$, is the canonical energy transfer from window 2 to window 1. The other two are usually very small. (For details, see [24]). It has been proved that $\Gamma^{0\to 1}$ is related to the instability in geophysical fluid dynamics [29]. Particularly, $\Gamma_A^{0\to 1}$ provides a quantitative measure of the baroclinic instability of the mean flow, while $\Gamma_K^{0\to 1}$ provides a barotropic instability measure. For convenience, in the following, we will write them as BC and BT, and may refer to them as baroclinic transfer and barotropic transfer, respectively. We hence have the following criterion:

If what we are considering are windows 0 and 1, then:

1. a flow is locally unstable if BT + BC >0, and vice versa;
2. for an unstable system, if BT > 0 and BC ≤ 0, the instability the system undergoes is barotropic;
3. for an unstable system, if BC > 0 and BT ≤ 0, then the instability is baroclinic; and
4. if both BC and BT are positive, the system must be undergoing a mixed instability.

If the windows in question are 1 and 2, the above criterion still works, but now the instability is with respect to the cyclone, which we will refer to as a secondary baroclinic/barotropic instability.

3. Data

The ERA-interim data with a horizontal resolution of $\mathbf{0.125}^\circ \times \mathbf{0.125}^\circ$, including temperature, geopotential, and wind (u, v, ω), will be used in this study to handle the dynamical processes involved in the cyclones. This reanalysis product is supplied by the European Centre for Medium-Range Weather Forecasts (ECMWF); vertically, it has 37 levels (from 1000 to 1 hPa) and the time resolution is 6 h. We choose a time span from July 1 to September 2, 2012, which covers the whole process of the typhoon Damrey and gives a time series of 256 steps, or $\mathbf{2^8}$

steps, as required by the analysis (We have seen in the preceding section that the number of steps should be a power of 2.)

4. MS-EVA setup

To set up the MS-EVA analysis, we first need to determine the window bounds j_0, j_1, *and* j_2. As shown above, the series has 2^8 steps, so $j_2 = 8$. To determine the other two scale levels, notice that although the duration of a tropical cyclone is generally 5–10 days, its life cycle from tropical turbulence at the cumulus convection scale to final decay may last more than 10 days. We have tried two lower bounds for the time scale levels—3 (corresponding to 16 days) and 2 (32 days). Through experiments, we find that $j_0 = 2$ gives a better cyclone separation, and hence will use this parameter for this study. The upper bound j_1 is chosen to be 7. That is to say, processes on time scales less than a day are regarded as cumulus convective disturbances. A summary of all other parameters is listed in **Table 2**.

Parameter	Value
Window bounds (j_0, j_1, j_2)	2, 7, 8 (corresponding to 32 days, 1 days, 6 h)
Horizontal grid	801 × 561
Spatial resolution	0.125°
Vertical levels	975, 950, 925, 900, 875, 850, 825, 800, 750, 700 650, 600, 550, 500, 450, 400, 350, 300, 250, 225 200, 175, 150, 125, 100, 70, 50, 30, 20, 10 hPa

Table 2. MS-EVA parameters.

5. Multiscale reconstructions

First we look at the reconstructions of the fields onto the three scale windows, i.e., the large-scale window, the cyclone window, and the convection window. Five pressure levels, 975, 850, 700, 500, and 300 hPa are selected for the illustration. They represent the boundary layer, the top of the boundary layer, lower, middle, and upper troposphere, respectively.

5.1. Large-scale flow

Figure 3 shows the original geopotential anomaly (left panel) and its large-scale reconstruction (right panel). Previously, it has been shown that, from late July to early August, in lower latitudes, the subtropical high lies further northward; in middle and high latitudes**,** the atmosphere at 500 hPa over East Asia is controlled by the Westerly in the south of a broad low with some short-wave troughs, while a ridge occupies aloft over the Seas of Okhotsk and Japan [30, 31]. **Figure 3** reconfirms this observation. On the 975 hPa level, the geopotential is characterized by low(s) in the west and high(s) in the east. The high pressure over the ocean is the

http://dx.doi.org/10.5772/intechopen.80018

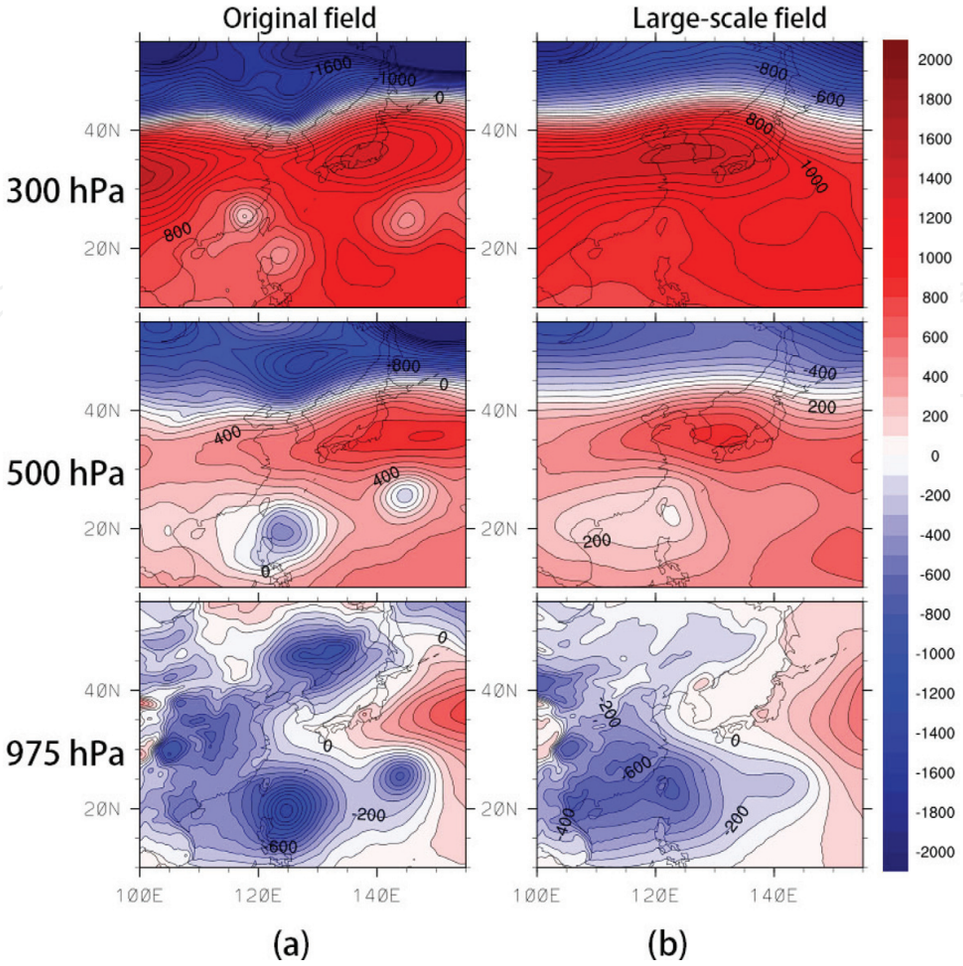

Figure 3. (a) The original geopotential ($m^2 \cdot s^{-2}$) and (b) its reconstruction on the large-scale window ($m^2 \cdot s^{-2}$) on July 30, 2012, at 975, 500, and 300 hPa.

subtropical high; around 30°N, there is a northwestern ridge. The low pressure covers the land, with intensity decreasing with height. The cyclones of the twin typhoon, Damrey and Saola, are clearly seen at all the levels shown. Damrey forms at the edge of the subtropical high; it then moves westward along the southern boundary. Saola has a different origin; it forms east of the Philippines, far from the subtropical high. It then moves northwestward and meets Damrey.

On the large-scale window (right panel in **Figure 3**), the low level (975 hPa) geopotential generally follows the original field, with a low in the west and a high in the east, but, differently, in middle and high latitudes, the interface separating the high and low is more along the land boundary, indicating the influence of the land. Over the West Pacific Warm Pool (WPWP), a low pressure sticks out eastward (centered around the island of Taiwan), and above the ocean at 30–37°N, east of 150°E, there is a high pressure center. In the lower troposphere, over the Sea of Japan is a low, but in the upper troposphere, a high center takes over the southern part of the Sea. North of 40°N, the region is mostly covered by low pressure. Generally, in the middle and upper troposphere, the large-scale geopotential is characterized by a high-pressure band between 25 and 35°N. That is to say, the subtropical high is narrow,

with a deep zonal easterly as its southern boundary; it lies farther in the north from bottom to the upper troposphere. This flow pattern provides the environment for Damrey's westward movement in higher latitudes.

A noteworthy feature on the large-scale geopotential anomaly map is the vertical dependence of the high- and low-pressure centers. From **Figure 3b**, the low weakens from 975 to 850 hPa, while the high strengthens from 500 to 300 hPa. The weakening of the low with height is due to the decreasing influence from the surface. We know a warm surface tends to cause a shallow warm low. In summer, both the warm land and the WPWP form warm surfaces, impacting together the form of the pressure field. For the subtropical high, it is more influenced by the downdraft branch of the Hadley cell, so there is a trend of strengthening with height. This results in a pattern above 700 hPa with a low in the north and a high in the south. Besides, the

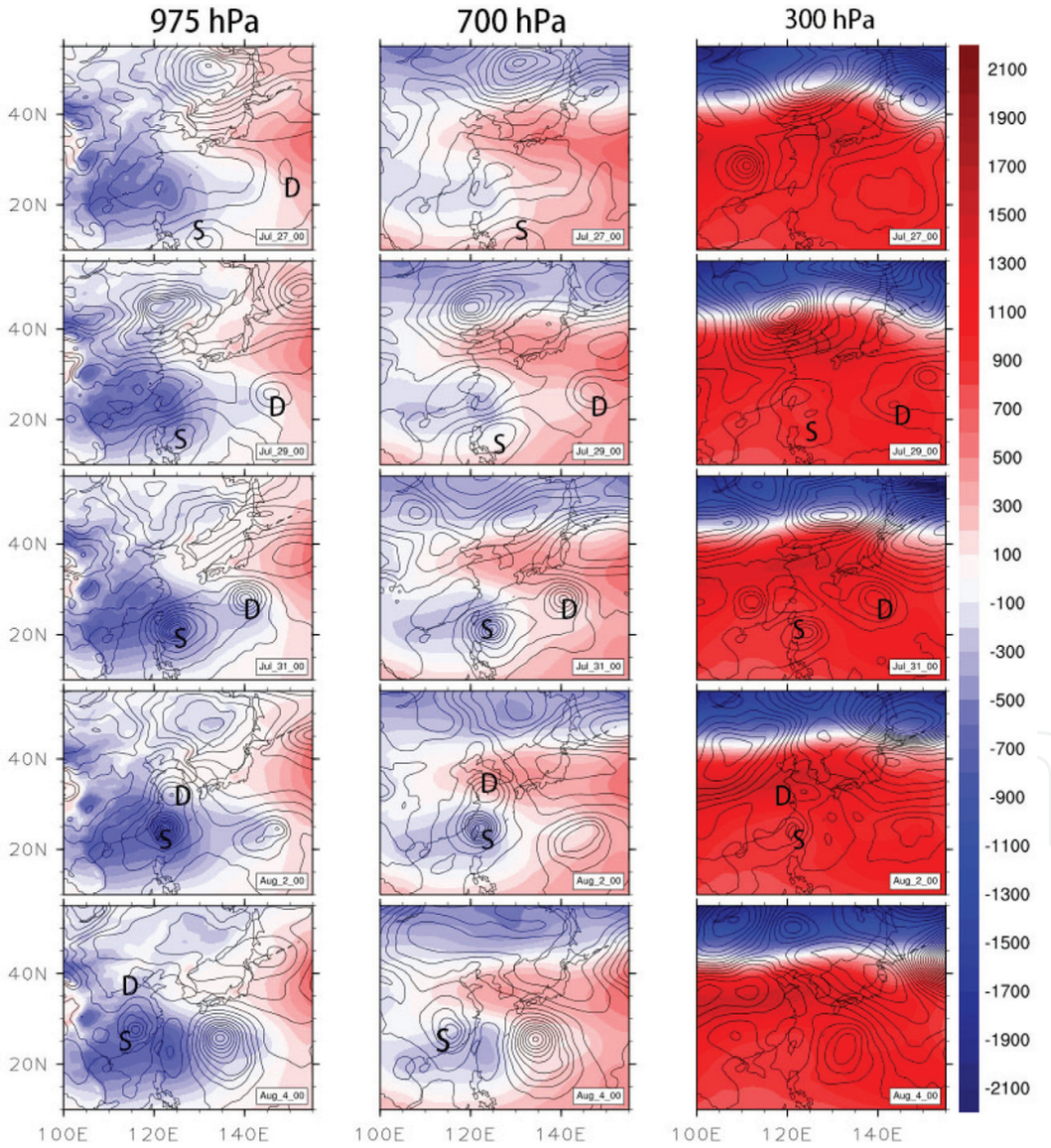

Figure 4. Geopotential anomaly ($m^2 \cdot s^{-2}$) on the cyclone window (contours) from July 27 to August 4, 2012, at 975, 700, and 300 hPa. The shaded background is the large-scale field.

South Asia high is clearly seen at 150 hPa (not shown), moving from the ocean to the Tibetan Plateau.

We remark that the large-scale field looks more like the climate state of the atmosphere. Many structures, the above vertical structure in particular, are largely disguised in the original field.

5.2. Cyclone-scale circulation

The cyclonic structures are reconstructed on the cyclonic window. Shown in **Figure 4** is the cyclone-scale geopotential anomaly (black solid line); for interpretation, also shown in the figure is the large-scale field (shaded). It is easy to see that both Damrey and Saola form at the interface between the low- and high-pressure regions, but in the original field, Saola is born far from the subtropical high. Initially, Damrey is weaker than Saola. After formation, the former moves westward along the interface, while latter moves northwestward to the low over Taiwan. They eventually hit the mainland of China in the north and south. The stronger Saola is then found to be weakened quickly, turning southwestward along the edge of the interface (This cannot be seen in the original field, either.)

For convenience, we define the birth time of a tropical cyclone as the time when the closed isopleths appear. By the criterion, both Damrey and Saola are first born in the lower troposphere: Damrey is born on July 27 at 0:00 at 975 and 850 hPa, while Saola is born before July 26. In the middle troposphere (700–500 hPa), Damrey appears slightly later (around 6:00, July 27). At 300 hPa and above, the scenario is quite different; a broad low occupies over the formation region.

By observation, the two cyclones last more than a week. At 975 hPa, the closed isopleths of Damrey completely disappear on August 4 at 12:00. At upper levels (e.g., 850, 700, and 500 hPa), Damrey dies on August 3 at 12:00 or earlier. In other words, Damrey not only appears more pronounced, but also lasts longer in the lower troposphere.

6. Canonical transfers and multiscale energetics

Among the multiscale energetics, the canonical transfers are pivotal to understanding the dynamics underlying the cyclogenesis of tropical cyclones. Different from the traditional transfer, which is a globally averaged quantity, it is a local notion, and hence can follow the cyclone's movement and trace its dynamical origin continuously. It has been validated with benchmark instability processes [29] and has been successfully applied to the study of many real atmosphere-ocean problems and engineering fluid problems. We will, henceforth, focus on these transfers and their evolutions. For convenience, the life cycle of Damrey is divided into three stages, namely, the stages of formation, maintenance, and decay.

6.1. Formation

The period between 0:00, July 27, and 0:00, July 31, is taken as the formation stage of Damrey. In this stage, the cyclone evolves from a tropical depression in the beginning, to a tropical storm at 0:00 July 28, and, eventually, to a strong tropical storm on July 31.

Figure 5 shows the canonical KE transfer, or barotropic transfer (BT) as called, between the large-scale window and cyclone window; a positive value indicates a transfer of energy from the basic flow to the cyclone, and the basic flow is hence unstable. Clearly, below 300 hPa, both cyclones have positive BT in the formation regions ($BT > 0$). By what is demonstrated in Section 2, the system is locally barotropically unstable. At 300 hPa, however, BT is quite differently distributed; in Damrey's birth place, BT is locally negative, i.e., the system is locally stable.

For the canonical KE transfer between the convection and cyclone windows, the scenario is different. As shown in **Figure 6**, it has not become significant until July 30. Around the typhoon Damrey, it gains KE from the convective processes ($-\Gamma_K^{1\to 2} > 0$) in the middle

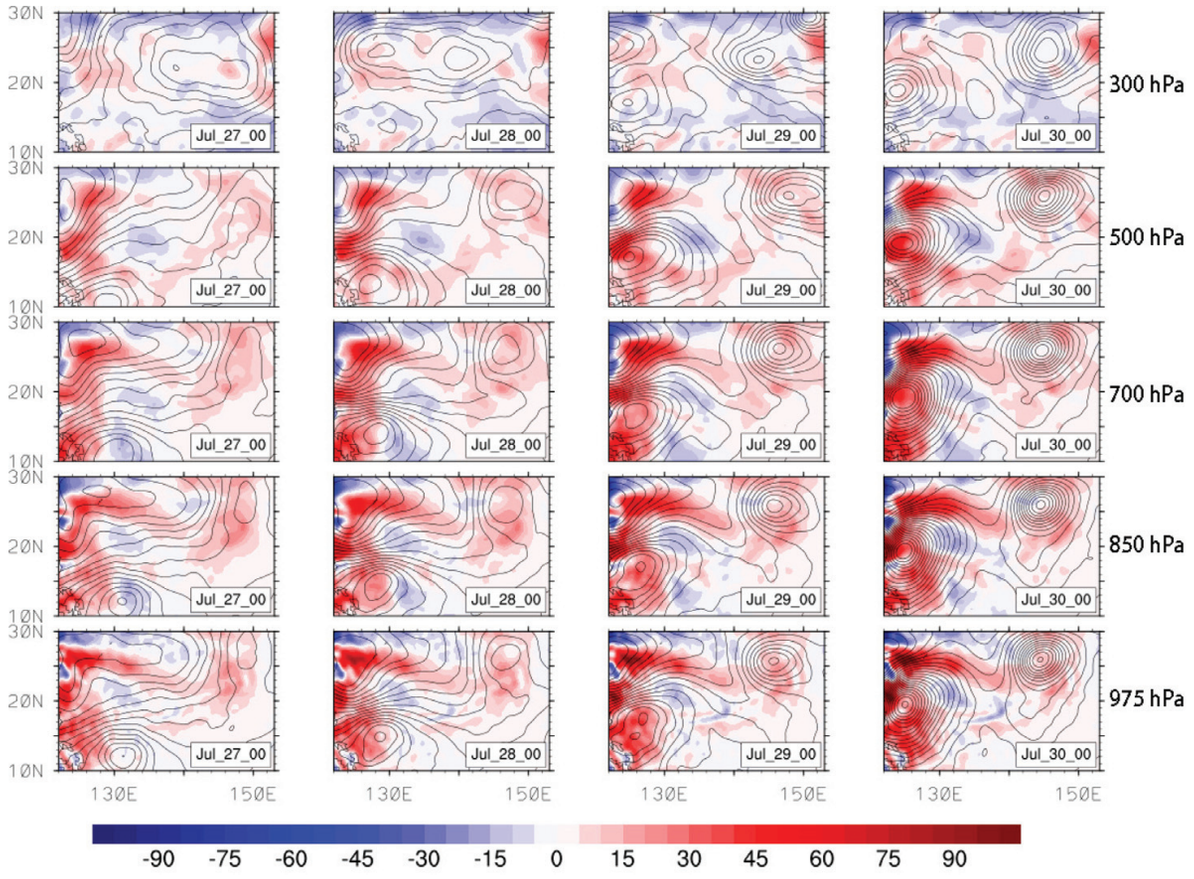

Figure 5. Canonical kinetic energy (KE) transfer ($10^{-5} \cdot m^2 \cdot s^{-3}$) between the large-scale and cyclone-scale windows from July 27 to July 30, 2012, at 975, 850, 700, 500, and 300 hPa. Shaded are the KE transfers between large-scale and cyclone-scale windows.(A positive value stands for a KE transfer from large-scale window to cyclone-scale window.) The red contour lines are the geopotential on the cyclone window; also superimposed are the cyclone-scale geopotential at 975 hPa (in black).

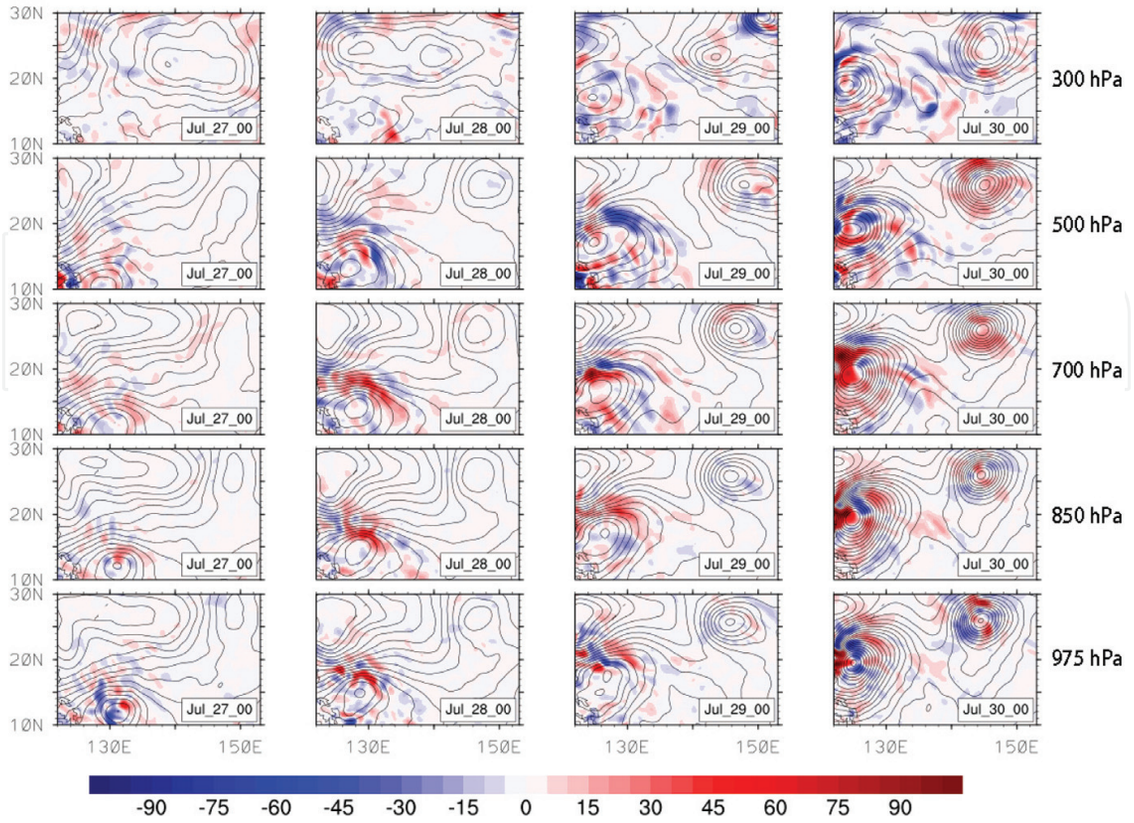

Figure 6. Same as **Figure 5**, but for canonical KE transfer ($10^{-5} \cdot m^2 \cdot s^{-3}$) between the convection and cyclone windows.

troposphere and loses KE ($-\Gamma_K^{1\to 2} < 0$) in the upper troposphere, though the gain and loss are both insignificant, in comparison with those between the basic flow and the cyclonic-scale window. Somehow, the cyclone provides a mechanism that takes the impact of the convective cumulus to the upper troposphere.

In contrast to its barotropic counterpart, the baroclinic transfer, or canonical APE transfer between the large-scale and cyclone windows, is insignificant in the lower troposphere (975–700 hPa). (The values over Taiwan are invalid because the highest altitude there is 3997 m.) Above 500 hPa (**Figure 7**), clear transfers can be seen in the formation region. Positive transfers (BC > 0), and hence baroclinic instabilities, exist over Taiwan and the Philippines. Particularly, to the east BC takes its maximum, while this is precisely where Saola will rapidly develop later. At 300 hPa, a baroclinic instability band lies between 15 and 25°N. But, this band does not cover the path that Damrey takes, except a protuberance at 147°E, 25°N, and hence does not contribute much to the cyclogenesis.

The ambient dynamical environments for the two tropical cyclones are similar. Upon generating, the local system around Saola is baroclinically unstable at 500 hPa and stable at 300 hPa. As it moves northwestward, it enters a baroclinic instability area aloft, which fuels its growth, with closed contour appearing on the geopotential field. It then slows down and intensifies rapidly in the region where BC attains its maximum, as shown above.

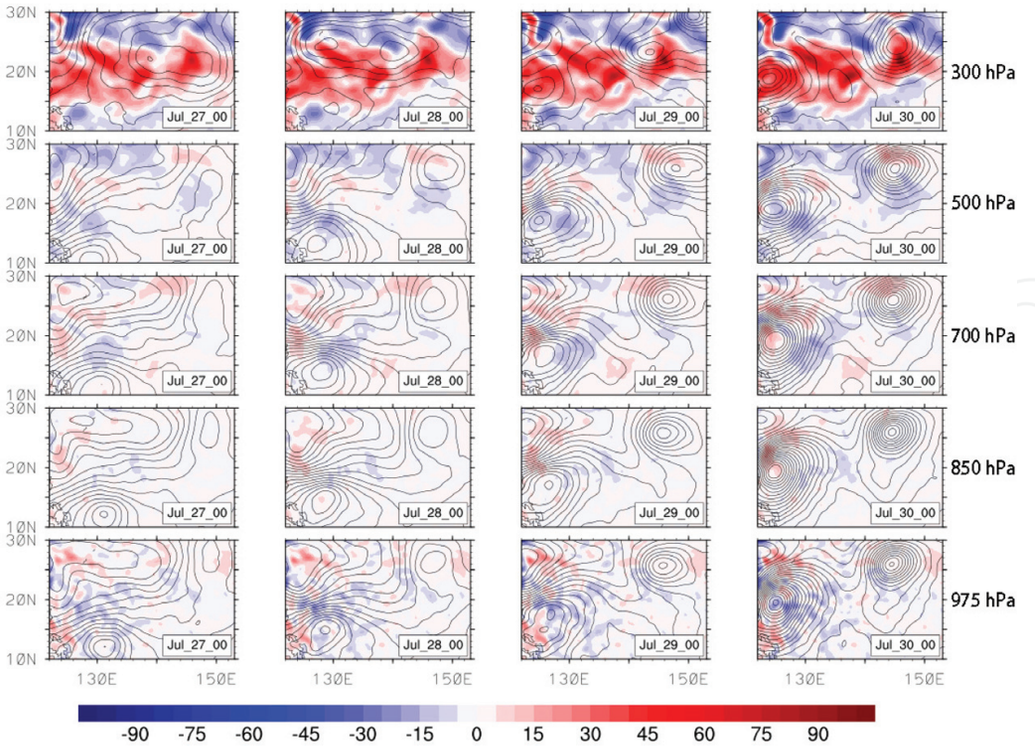

Figure 7. Same as **Figure 5**, but for canonical APE transfer ($10^{-5} \cdot m^2 \cdot s^{-3}$) at 500 and 300 hPa.

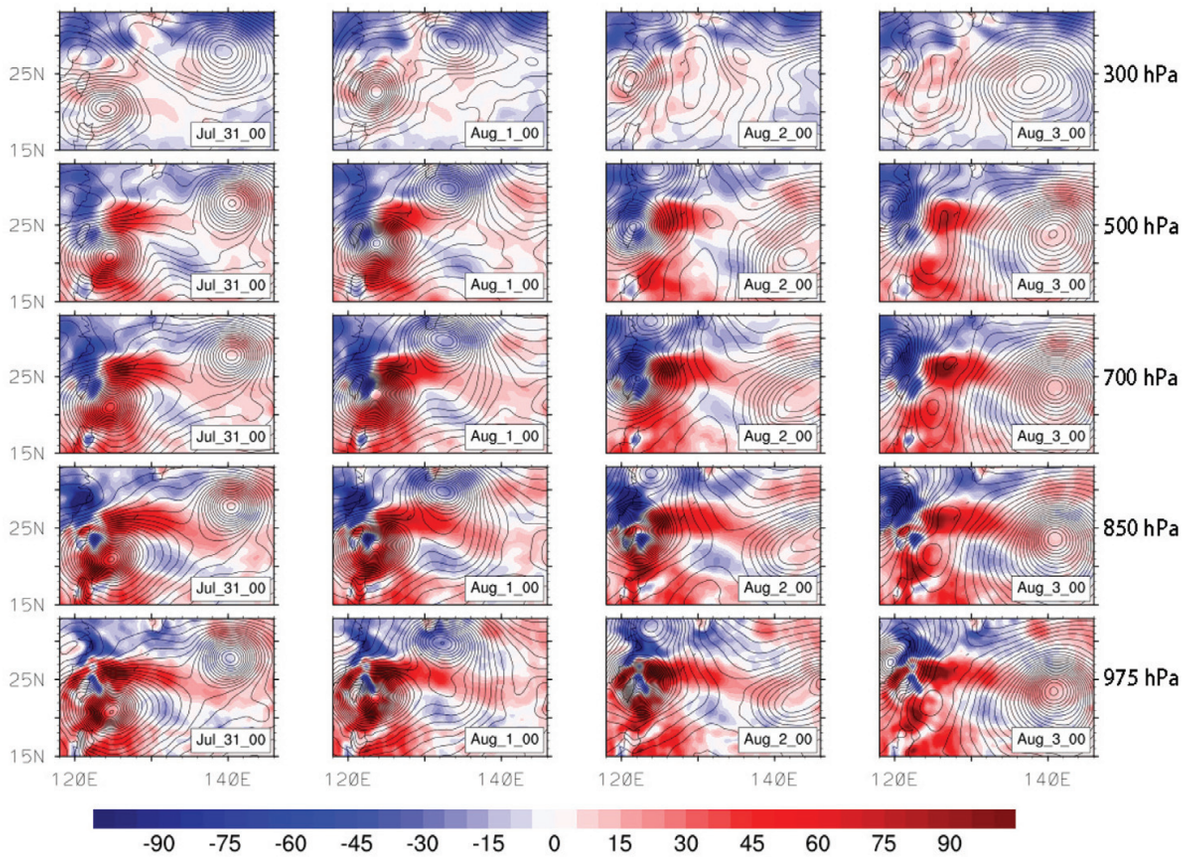

Figure 8. Same as **Figure 5** but from July 31 to August 3, 2012.

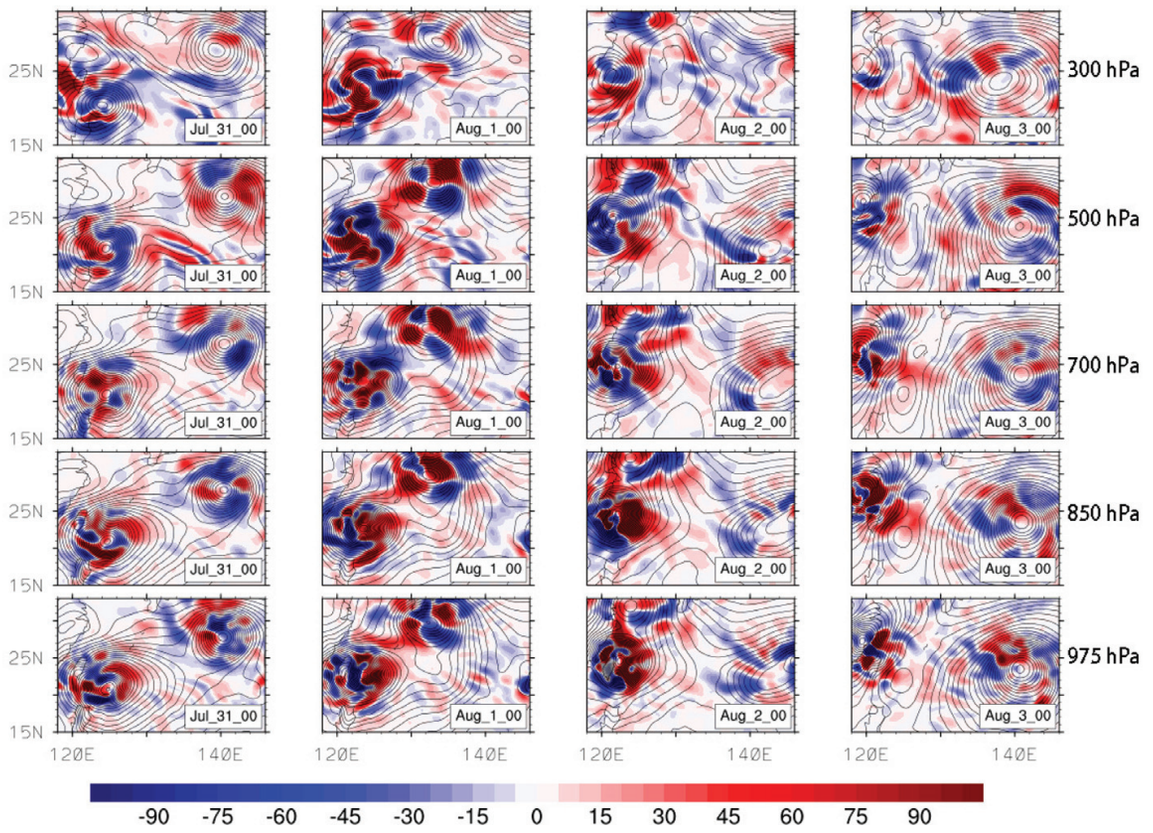

Figure 9. Same as **Figure 6** but from July 30 to August 3, 2012.

Damrey has gone through similar dynamical processes. In the beginning, it forms in a region, which is baroclinically unstable at 500 hPa and stable at 300 hPa. It moves westward and becomes strengthened at lower levels beneath that protuberance of the baroclinically unstable band (formed since July 28). The canonical APE transfer between the cyclone and convection windows is rather weak and does not make significant contribution.

6.2. Maintenance and rapid development

After the formation, Damrey actually experiences another intensification (since July 31), which eventually makes it a strong tropical storm. After August 1 at 12:00, it goes into a stage of rapid development until August 2 at 6:00.

As shown in **Figure 8**, after the cyclones are formed, the canonical KE transfer between the large-scale and cyclonic-scale windows takes a pattern of inverse cascade (BT < 0) in the north and barotropic instability (BT > 0) in the south. From 975 to 500 hPa, the inverse cascade region spreads southward and westward. At 300 hPa, a wide region of negative BT appears north of 30°N. During this period along the track of Damrey, the troposphere is barotropically stable (BT < 0).

For the canonical KE transfers between convection and cyclone windows (**Figure 9**), they mainly show up around the cyclones, with intensity positively related to the strength of the cyclones. From the figure, secondary instabilities and stabilities lie alternatively. By their

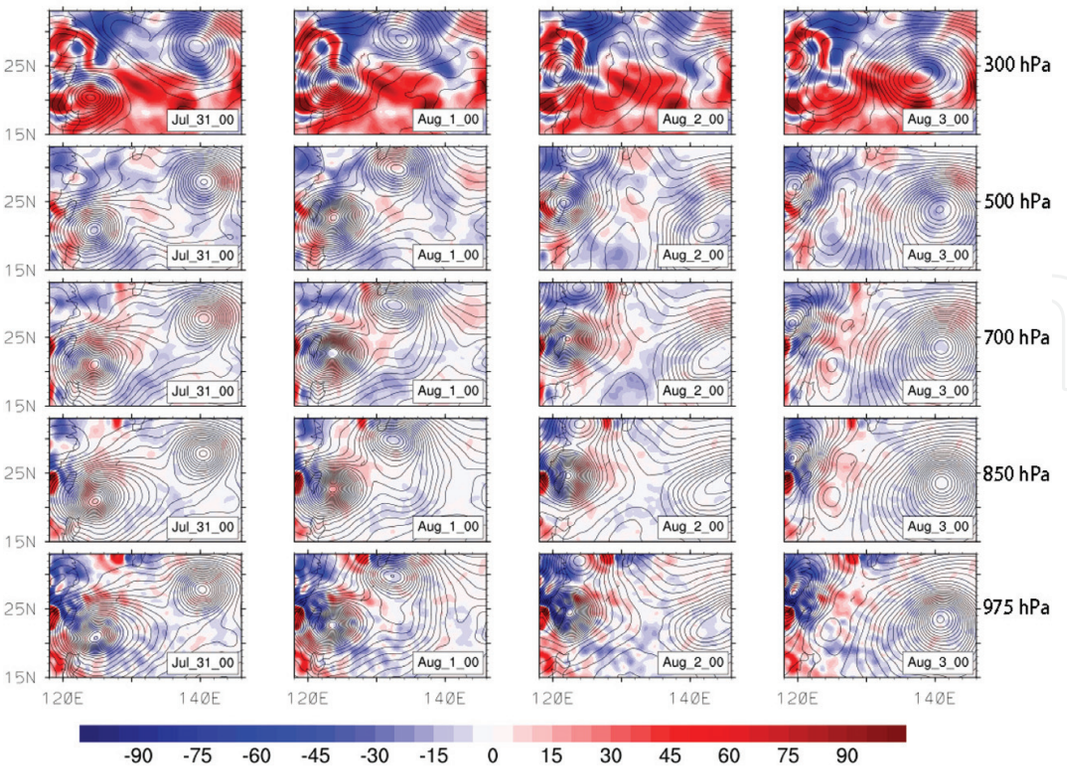

Figure 10. Same as **Figure 7**, but at 975, 850, 700, 500, and 300 hPa from July 31 to August 3, 2012.

magnitudes and distribution pattern, the convection-scale processes may not serves as energy sources or sinks to the cyclone.

The canonical APE transfers in the stage of maintenance are displayed in **Figure 10**. Obviously, at 850 hPa, the atmosphere east of the China mainland is baroclinically stable (BC < 0), but in the coastal region north of 25°N, there exist baroclinic instabilities. Below 500 hPa, the canonical transfer rate decreases with height. In the upper troposphere (300 hPa), the atmosphere is baroclinically unstable (BC > 0) over the mainland north of 25°N. But BC is still negative over the sea, to the east of Yangtze River's estuary, and to the south of Japan. That is to say, the baroclinic canonical transfer is rather unfavorable Damrey. This situation makes a slight difference for Saola. The positive baroclinic transfer over the sea above 500 hPa tends to facilitate Saola.

The canonical APE transfer between the convection and cyclone windows is rather weak below 500 hPa. But at 300 hPa, there exists a center of positive transfer to the convective window, indicating a secondary instability of the cyclonic-scale process.

6.3. Decay

On August 2 at 6:00, Damrey starts to decay, though it has not landed yet. Although it is argued that the dissipative/diffusive processes cause a perturbed atmosphere to resume to its original state, here, the decay of Damrey has its dynamical origin from within the atmosphere

itself. Generally, barotropic transfer seems to be unfavorable to its maintenance. A conspicuous feature of **Figure 5** is the existence of an inverse cascade region near the mouth of Yangtze River (outside Shanghai). Upon entering the region on August 2 at 6:00, Damrey stops growing and decays rapidly after it lands onto Jiangsu. Similarly, a local inverse baroclinic cascade over Fujian and Taiwan may cause the decay of Saola after its landing.

Note that when Damrey and Saola land, they are close to each other. As argued in Guinn and Schuber [32], two vortices will interact when getting together, with the strong one annihilating the weak one. The final decay of Damrey could be related to this kind of interaction mechanism; a discussion of it, however, is beyond the scope of this study.

7. Concluding remarks

In late July-early August 2012, a devastating typhoon, Damrey, landed on Jiangsu, the populous coastal province of China, causing severe flooding and other disasters in East China. Damrey is special in that it is of higher latitude origin, and, besides, it forms a part of a twin typhoon (another part is Saola). In this study, we investigated the multiscale dynamical processes that lead to the formation, maintenance, and decay of the phenomenon, using a newly developed functional analysis tool, multiscale window transfer (MWT), and the MWT-based localized multiscale energy and vorticity analysis (MS-EVA).

We first reconstructed the atmospheric fields onto three orthogonal subspaces, namely, the large-scale window, tropical cyclone-scale window, and cumulus convection-scale window, and then diagnosed the local Lorenz cycles among them. Based on the results, the two cyclones form in the lower troposphere due to some barotropic instabilities. To be specific, we have identified a pronounced area of barotropic instability in the region of 145–150°E, 20–25°N, and, remarkably, it corresponds to the birthplace of the tropical depression—the Damrey in its infant stage. The initial disturbance receives kinetic energy (KE) from the large-scale basic flow in lower troposphere and develops upward. This agrees with Duan and Wu [20], who found that barotropic transfers make significant contribution to the tropical cyclones generated at the confluence region of and inside the monsoon trough. It also agrees with Maloney [12] who concluded that during the formation stage of a tropical cyclone, eddy kinetic energy mainly comes from the large-scale circulation. In other words, the initial formation has little relation to baroclinic processes. In fact, Damrey receives available potential energy (APE) from the large-scale window in middle levels (700–500 hPa), and returns it to the same window at 300 hPa. But on the whole, the net canonical APE transfer between the large-scale and cyclone windows is insignificant, suggesting that Damrey's birth is not caused by accumulating of APE.

But the further developments of Damrey and its peer Saola are indeed related to baroclinic processes and, particularly, baroclinic instabilities in the upper troposphere. Their rapid intensifications after formation both happen at the strong baroclinic instability areas in the middle and upper troposphere. Nonetheless, the canonical transfers after formation are, in general, rather unfavorable to the maintenance of Damrey, especially the negative transfer over the East China Sea outside Shanghai (at the mouth of Yangtze River). The intense barotropic and

baroclinic inverse cascades are responsible for the rapid decay of Damrey before landing. But since at this time, its twin counterpart is just nearby, the final decay of Damrey is likely to be related to the interaction with Saola, a mechanism we leave to future studies.

It merits mentioning that the energetic scenario during the cyclogenesis of Damrey has a distinct vertical structure. We have seen from the analysis above that Damrey gets KE from the large-scale flow in the lower troposphere (below 500 hPa) and loses KE to the large-scale window and the convection window above. This explains why Damrey forms from lower to higher levels. Also, this is in accordance with Zhang and Bao [33], who proposed a "bottom-up hypothesis": deep convection will develop from bottom to top under the organization of mesoscale convective vortices (MCV) and lead to the formation of tropical cyclones.

The cumulus convection has been said to play a role in tropical cyclogenesis (e.g., [3]). In this study, however, the transfer between the convection and cyclone windows is always weak, implying that cumulus convections do not serve as an energy source, agreeing with air-sea interaction theory by Emanuel [34, 35], who argues that cumulus convections only function to transport energy rather than provide energy source in tropical cyclone formation. However, his hypothesis that the energy source be moisture entropy (estimated with equivalent potential temperature in his papers) from the underlying ocean is yet to be verified. In this special case, as we have seen before, Damrey forms as energy is extracted through a barotropic instability from the background flow. That is to say, the background flow provides the needed energy source. We hope to verify the existing theories of cyclogenesis in more case diagnoses with the new methodology.

Acknowledgements

Thanks are due to ECMWF for the ERA-interim data and to CMA for the track data. This study was partially supported by the Jiangsu Provincial Government through the 2015 Jiangsu Program for Entrepreneurship and Innovation Group and the Jiangsu Chair Professorship, by the National Science Foundation of China (NSFC) under Grant 41276032 and by the State Oceanic Administration through the National Program on Global Change and Air-Sea Interaction (GASI-IPOVAI-06).

Author details

X. San Liang[1,2]* and Lan Wang[1]

*Address all correspondence to: x.san.liang@gmail.com

1 School of Atmospheric Sciences, Nanjing University of Information Science and Technology, Nanjing, China

2 School of Marine Sciences, Nanjing University of Information Science and Technology, Nanjing, China

References

[1] Gray WM. Global view of the origin of tropical disturbances and storms. Monthly Weather Review. 1968;**96**:87

[2] Wang L, Liang XS. A diagnosis of some dynamical processes underlying a higher-latitude typhoon using the multiscale window transform. Atmosphere. 2017;**8**:118. DOI: 10.3390/atmos8070118

[3] Cheung KKW. Large-scale environmental parameters associated with tropical cyclone formations in the western north pacific. Journal of Climate. 2010;**17**:466-484

[4] Landsea CW. A climatology of intense (or major) atlantic hurricanes. Monthly Weather Review. 1993;**121**:1703

[5] Molinari J, Vollaro D, Skubis S, Dickinson M. Origins and mechanisms of eastern pacific tropical cyclogenesis: A case study. Monthly Weather Review. 2000;**128**:2010

[6] Li XY, Wu LG, Zong HJ. Analysis of influence of monsoon gyres on tropical cyclogenesis over the western North Pacific. Transactions of Atmospheric Sciences. 2014;**37**:653-664. (in Chinese)

[7] Qiu WY, Wu LG. Influence of north-west Pacific monsoon depression on tropical cyclogenesis. Chinese Journal of Atmospheric Sciences. 2015;**35**:237-247. (in Chinese)

[8] Ritchie EA, Holland GJ. Large-scale patterns associated with tropical cyclogenesis in the western Pacific. Monthly Weather Review. 1999;**127**:2027-2043

[9] Zhang WL, Zhang DL, Wang AS, Cui XP. An investigation of the genesis of typhoon Durian (2001) from a monsoon trough. Acta Meteorologica Sinica. 2008;**67**(5):811-827. (in Chinese)

[10] Zong HJ, Wu LG. Re-examination of tropical cyclone formation in monsoon troughs over the western North Pacific. Advances in Atmospheric Sciences. 2015;**32**:924-934

[11] Maloney ED, Hartmann DL. Modulation of hurricane activity in the gulf of Mexico by the Madden-Julian oscillation. Science. 2000;**287**:2002-2004

[12] Maloney ED, Hartmann DL. The Madden-Julian oscillation, barotropic dynamics, and North Pacific tropical cyclone formation. Part I: Observations. Journal of the Atmospheric Sciences. 2001;**58**:2545-2558

[13] Sun Z, Mao JY, Wu GX. Influences of intraseasonal oscillations on the clustering of tropical cyclone activities over the western North Pacific during boreal summer. Chinese Journal of Atmospheric Sciences. 2009;**33**:950-958. (in Chinese)

[14] Zhu CW, Nakazawa T, Li JP. Modulation of tropical depression/cyclone over the Indian-Western Pacific oceans by Madden-Julian oscillation. Chinese Journal of Atmospheric Sciences. 2004;**62**:42-50. (in Chinese)

[15] Mcbride JL, Keenan TD. Climatology of tropical cyclone genesis in the Australian region. International Journal of Climatology. 1982;**2**:13-33

[16] Montgomery MT, Farrell BF. Tropical cyclone formation. Journal of the Atmospheric Sciences. 1993;**50**:285-308

[17] Sadler JC. A role of the tropical upper tropospheric trough in early season typhoon development. Monthly Weather Review. 1974;**104**:57

[18] Ooyama KV. Conceptual evolution of the theory and modeling of the tropical cyclone. Journal of the Meteorological Society of Japan. Ser. II. 1982;**60**:369-380

[19] Papin P. Using the Rossby radius of deformation as a forecasting tool for tropical cyclogenesis. In: Proceedings of the National Conference on Undergraduate Research; 31 March-2 April 2011; Ithaca, NY, USA

[20] Duan JJ, Wu LG. Kinetic energy budget analysis of tropical cyclogenesis precursors in the monsoon trough. Chinese Journal of Atmospheric Sciences. 2016;**36**:141-148. (in Chinese)

[21] Batchelor GK. The Theory of Homogeneous Turbulence. Cambridge: Cambridge University Press; 1953

[22] Strang G, Nguyen T. Wavelets and Filter Banks. Wellesley: Wellesley-Cambridge Press; 1996

[23] Liang XS, Anderson DGM. Multiscale window transform. SIAM Journal on Multiscale Modeling & Simulation. 2007;**6**:437-467

[24] Liang XS. Canonical transfer and multiscale energetics for primitive and quasi-geostrophic atmospheres. Journal of the Atmospheric Sciences. 2016;**73**:4439-4468. DOI: 10.1175/JAS-D-16-0131.1

[25] Liang XS, Robinson AR. Localized multiscale energy and vorticity analysis: I. Fundamentals. Dynamics of Atmospheres and Oceans. 2005;**38**(3):195-230

[26] Pope SB. Turbulent Flows. Cambridge: Cambridge University Press; 2004. p. 771

[27] Holopainen EO. A diagnostic study on the kinetic energy balance of the long-term mean flow and the associated transient fluctuations in the atmosphere. Geophysica. 1978;**15**:125-145

[28] Plumb RA. A new look at the energy cycle. Journal of the Atmospheric Sciences. 1983;**40**: 1669-1688. 1669: ANLATE.2.0.CO;2. DOI: 10.1175/1520-0469(1983)040

[29] Liang XS, Robinson AR. Localized multi-scale energy and vorticity analysis: II. Finite-amplitude instability theory and validation. Dynamics of Atmospheres and Oceans. 2007;**44**:51-76

[30] Tao YW. Analysis of the August 2012 atmospheric circulation and weather. Meteorological Monographs. 2012;**28**(11):1429-1435. (in Chinese)

[31] Zhou NF. Analysis of the July 2012 atmospheric circulation and weather. Meteorological Monographs. 2012;**38**(10):1307-1312. (in Chinese)

[32] Guinn TA, Schubert WH. Hurricane spiral bands. Journal of the Atmospheric Sciences. 1993;**50**:3380

[33] Zhang DL, Bao N. Oceanic cyclogenesis as induced by a mesoscale convective system moving offshore. Part II: Genesis and thermodynamic transformation. Monthly Weather Review. 1996;**124**:2206

[34] Emanuel KA. An air-sea interaction theory for tropical cyclones. Part I: Steady-state maintenance. Journal of the Atmospheric Sciences. 1986;**43**:585-605

[35] Emanuel KA. The theory of hurricanes. Annual Review of Fluid Mechanics. 2003;**23**:179-196

IntechOpen